Available online at www.sciencedirect.com
ScienceDirect
Neurocomputing 70 (2007) 1390–1402
NEUROCOMPUTING
www.elsevier.com/locate/neucom

A biophysical neural accumulator model of decision making in an antisaccade task

Vassilis Cutsuridis[a,*], Ioannis Kahramanoglou[a], Nikolaos Smyrnis[b,c], Ioannis Evdokimidis[b], Stavros Perantonis[a]

[a]*Computational Intelligence Laboratory, Institute of Informatics and Telecommunications, National Center for Scientific Research "Demokritos", Agia Paraskevi, Athens GR-15310, Greece*
[b]*Cognition and Action Group, Neurology Department, National University of Athens, Aeginition Hospital, 72 Vas Sofias Ave., Athens GR-11528, Greece*
[c]*Psychiatry Department, National University of Athens, Aeginition Hospital, 72 Vas Sofias Ave., Athens GR-11528, Greece*

Received 4 September 2005; received in revised form 19 May 2006; accepted 7 June 2006
Available online 10 October 2006

Abstract

A biophysical cortico-colicular model of saccade initiation based on competitive integration of planned and reactive cortical saccade decision signals in the intermediate layer of the superior colliculus is introduced. The variable slopes of the climbing activities of the input cortical decision signals are produced from variability in the ionic and synaptic conductances of cortical neurons. The model reproduces the unimodal distributions of saccade reaction times for correct antisaccades and erroneous prosaccades as well as the variability of saccade reaction times and the overall error probabilities in a large sample of 2006 young men performing an antisaccade task.

Keywords: Climbing activity; Antisaccade; Decision making; Superior colliculus; Computational model

1. Introduction

The antisaccade task is a reaction time (RT) task in which the subjects are instructed to perform eye movements in the opposite direction from the location of a stimulus that appears in their left or right peripheral visual field while they are fixating on a central stimulus [22]. The antisaccade reaction times (aSRTs) have been reported to be longer than those in the reflexive saccades (prosaccades) and to vary randomly from trial-to-trial and both between subjects and within subjects [19]. The distribution of aSRTs is unimodal and the percentage of erroneous prosaccades towards the peripheral stimulus is 25% [16,43].

In a modeling attempt of the antisaccade task, Cutsuridis and colleagues [10,11] hypothesized that the preparation of an antisaccadic eye movement consisted of two cortically independent and spatially separated decision signals representing the reactive and planned saccade signal, whose linearly rising phases were derived from two normal distributions with different means and standard deviations. These two cortical decision signals were integrated at opposite colliculi locations, where they competed against each other via lateral excitation and remote inhibition. A saccade was initiated when these decision signals, represented by the neuronal activity of superior colliculus (SC) buildup neurons with non-linear growth rates reached a preset criterion level. The crossing of the preset criterion level in turn released the "brake" from the SC burst neurons and allowed them to discharge resulting in the initiation of an eye movement. The model's main prediction was that there was no need of a top-down inhibitory signal that prevented the error prosaccade from being expressed, thus allowing the correct antisaccade to be released [7]. Moreover, the model simulated successfully responses of fixation neurons [34], buildup neurons [18,33,35,36] and burst neurons [18,35,36,48] and offered a functional rationale at the SC neuronal population level

*Corresponding author. Tel.: +30 210 6503175; fax: +30 210 6532175.
E-mail address: vcut@iit.demokritos.gr (V. Cutsuridis).

0925-2312/$ - see front matter © 2006 Elsevier B.V. All rights reserved.
doi:10.1016/j.neucom.2006.06.002

of why the antisaccadic RTs were long and variable. Finally, the model simulated accurately the correct and error antisaccade RTs, the RT shape distributions and the error prosaccade probabilities in a population sample of 2006 men [16,43].

The model presented in this paper extends the previous model of Cutsuridis and colleagues [10,11] by examining the biophysical mechanisms that cause the variability in the rising phases of the two cortical decision signals in the SC model. It does so by adding two cortical modules that generate the reactive and planned decision signals (see Fig. 1) that drive the SC model. The activities of the two cortical modules are derived from the population activities of networks of pyramidal neurons and inhibitory interneurons. Hodgkin–Huxley mathematical formulations are used to model the population activities and explore the biophysical mechanisms in question. The present model predicts that variability in the maximal conductances of specific ionic and synaptic currents (see Results section for which currents and their corresponding values) can reproduce the full range of slope values (see Table 4) of the planned and reactive inputs of the SC model [10,11], while keeping the preset criterion level fixed. By reproducing the full range of the slope values, the model can implicitly generate the correct antisaccade and the error prosaccade RT distributions as well as the error prosaccade probabilities in the large group of 2006 men [16,43] published elsewhere [10,11].

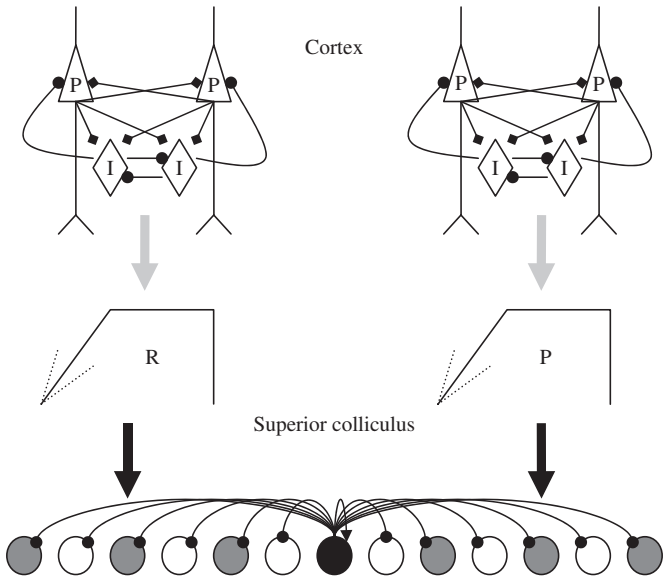

Fig. 1. Composite model architecture of cortical modules and superior colliculus module with reactive and planned inputs. Cortex: triangular neurons symbolize pyramidal cells and diamond shaped neurons symbolize GABAergic inhibitory inteneurons. Superior colliculus: black nodes are fixation cells, gray nodes are buildup cells, and white nodes are burst cells. The inputs to this layer are classified as reactive (R) and planned (P). Their respective time course is shown schematically corresponding to an onset and offset.

2. Materials and methods

2.1. Cortical model neuron

Each pyramidal neuron is described by a single compartment and obeys the current balance equation

$$C_p \frac{dV_p}{dt} = -I_L - I_{Na} - I_{NaP} - I_{HVA} - I_{Kd} - I_C - I_{Ks} - I_{AHP} - I_{AMPA} - I_{NMDA} - I_{GABA} + I_{inj}, \quad (1)$$

where $C_p = 1.2\,\mu F/cm^2$ and I_{inj} is the injected current (in $\mu A/cm^2$). Similarly, each inhibitory interneuron is also described by a single compartment and obeys the current balance

$$C_{inh} \frac{dV_{inh}}{dt} = -I_L - I_{Na} - I_{Kd} - I_{AMPA} - I_{NMDA} - I_{GABA} + I_{inj}, \quad (2)$$

where $C_{inh} = 1.2\,\mu F/cm^2$. The leak current $I_L = g_L(V–E_L)$ in Eqs. (1) and (2) has a conductance $g_L = 0.02\,mS/cm^2$ and reversal potential $E_L = -65\,mV$.

The voltage-dependent currents are described by Hodgkin–Huxley formalism [25]. Each gating variable x is described by a first order kinetics

$$\frac{dx}{dt} = \alpha_x(V)(1-x) - \beta_x(V)x = [x_\infty(V) - x]/\tau_x(V). \quad (3)$$

The fast sodium current in Eqs. (1) and (2) is governed by$I_{Na} = \bar{g}_{Na} m^3 h(V - E_{Na})$, where the activation variable, m, is replaced by its steady state, $m_\infty = \alpha_m/(\alpha_m + \beta_m)$, $\alpha_m = [-0.1(V+33)]/[-1 + \exp(-0.1(V+33))]$ and $\beta_m = 4\exp(-(V+58)/12)$. The inactivation variable, h, obeys Eq. (3), where $h_\infty = \alpha_h/(\alpha_h + \beta_h)$, $\tau_h = 1/(\alpha_h + \beta_h)$, $\alpha_h = 0.07\exp(-(V+50)/10)$ and $\beta_h = 1/[1 + \exp(-0.1(V+20))]$.

In addition to the fast sodium current, a delayed rectifier potassium current is included in both Eqs. (1) and (2) to counteract the sodium current's effect on cell's membrane potential. The delayed rectifier is given by,$I_{Kd} = \bar{g}_{Kd} n^4 (V - E_{Kd})$, where $\alpha_n = [-0.01(V+34)]/[-1 + \exp(-0.1(V+34))]$ and $\beta_n = 0.125\exp(-(V+44)/25)$ [49].

A persistent Na^+ current (I_{NaP}) is also included in the current balance equation of the pyramidal neuron in order to allow the more persistent Na^+ current to make a more significant contribution to the membrane potential in the subthreshold level [2,4]. The persistent Na^+ current is given by, $I_{NaP} = \bar{g}_{NaP} mh(V - E_{NaP})$, where $m_\infty = \alpha_m/(\alpha_m + \beta_m)$, $\tau_m = 1/(\alpha_m + \beta_m)$, $\alpha_m = [-0.2816(V+12)]/[-1 + \exp(-(V+12)/9.3)]$, $\beta_m = [0.2464(V-15)]/[-1 + \exp((V-15)/6)]$, $h_\infty = \alpha_h/(\alpha_h + \beta_h)$, $\tau_h = 1/(\alpha_h + \beta_h)$, $\alpha_h = 2.8 \times 10^{-5}\exp(-(V + 42.8477)/4.02)$ and $\beta_h = 0.02/[1 + \exp(-(V - 413.9284)/148.26)]$. The conductance $g_{NaP} = 1\,mS/cm^2$ and the reversal potential $E_{NaP} = +55\,mV$ [15]. The persistent Na^+ current has been found to exist in cortical pyramidal cells due to its sensitivity with TTX [4]. This current is activated within a few ms after depolarization, but it inactivates very slowly. Because it is activated near the resting potential, it tends to amplify EPSPs [4]. Finally,

it has quite an effect on the firing frequency of the cell, since too much I_{NaP} will prevent repolarization following action potentials [31].

The high-voltage activated (HVA) calcium current included in Eq. (1) is considered to be a mixture of L- and N-type Ca^{2+} currents, which according to [3] have the same activation kinetics. The HVA calcium current is expressed by $I_{HVA} = \bar{g}_{HVA} m_\infty (V - E_{HVA})$, where $m_\infty = [1 + \exp(-(V + 20)/9)]^{-1}$ [30].

The afterhyperpolarizing calcium-activated potassium current is given by $I_{sAHP} = g_{sAHP}([Ca^{2+}]/([Ca^{2+}] + K_D))(V - E_{sAHP})$ with $K_D = 30\,\mu M$ [49]. The intracellular calcium concentration $[Ca^{2+}]$ is governed by a first order differential equation

$$\frac{d[Ca^{2+}]}{dt} = -\gamma I_{AHP} - \frac{([Ca^{2+}] - [Ca^{2+}]_{rest})}{\tau_{Ca,AHP}}, \quad (4)$$

where $\gamma = 0.002\,\mu M\ (mS\,\mu A)^{-1}\,cm^2$ is proportional to the membrane area and the volume beneath the membrane [49]. The time constant $\tau_{Ca,AHP} = 70\,ms$ describes collectively the various extrusion and buffering mechanisms [51]. The AHP current has been characterized as a rather small current, which depends solely on the concentration of intracellular calcium just below the membrane. It can sustain its activation only when calcium rushes into the cell during an action potential [32]. Blocking this current prevents firing frequency adaptation from occurring [31].

A fast BK Ca^{2+}- and voltage dependent C-type K^+ current (I_C) is also included in the model. In contrast with the AHP current, the I_C current is a fairly large outward current, whose activity depends on the membrane potential as well as the intracellular Ca^{2+} concentration [32]. It quickly activates upon the entry of calcium through calcium channels during an action potential and through this process it shuts off the readiness for the next spike [32]. The biophysical properties of this current used herein were adopted from [15]. The $I_C = \bar{g}_{fC} c^2 (V - E_C)$, where c obeys Eq. (3) with $c_\infty = \alpha_c/(\alpha_c + \beta_c)$, $\tau_c = \max(1/(\alpha + \beta), 1.1)$, $\alpha_c = -0.00642 V_s - 0.1152]/[-1 + \exp(-(V_s + 18)/12)]$, $V_s = V + 40\log_{10}([Ca]_i)$ and $\beta_c = 1.7\exp(-(V_s + 152)/30)$. The intracellular calcium concentration obeys Eq. (4), with $\tau_{Ca,C} = 10\,ms$. Notice that the time constant values for I_C and I_{AHP} are different. We have assumed that two different Ca^{2+} ionic pools exist, one mediating the activation of I_{AHP} and the other one mediating the activation of I_C. The rationale behind such an assumption is that the internal Ca^{2+} concentration affecting I_C rises and falls fairly rapidly with every spike, whereas the internal Ca^{2+} concentration affecting I_{AHP} increases gradually after each action potential [51].

A slowly inactivating K^+ current (I_{Ks}) is also present in pyramidal neurons. Activation of this slowly inactivating outward K^+ current shunts excitatory inputs and hence prevents a cell from reaching spike threshold [3]. The formulation of I_{Ks} is taken from [15]. More specifically, $I_{KS} = \bar{g}_{KS} ab (V - E_{KS})$, where $a_\infty = 1/[1 + \exp(-(V + 34)/6.5)]$, $\tau_a = 6.0$, $b_\infty = 1/[1 + \exp((V + 65)6.6)]$ and $\tau_b = 200 + 3200/[1 + \exp(-(V + 63.6)/4)]$. The values of the ionic parameters are displayed in Tables 1 and 2. The ionic channels steady-state and time-constant curves are shown in Fig. 2.

2.2. Cortical model synapse

The synaptic current is given by $I_{syn} = g_{syn} s (V - E_{syn})$, where g_{syn} is the maximal synaptic conductance and E_{syn} is the reversal potential. In the model, three synaptic currents are included: I_{AMPA}, I_{NMDA} and $I_{GABA\text{-}A}$. The values of the synaptic parameters are displayed in Table 3. The gating variable s, which represents the fraction of open synaptic ion channels, obeys the following differential equation [12,38]

$$\frac{ds}{dt} = \alpha F(V_{pre})(1 - s) - \beta s, \quad (5)$$

Table 1
Parameter profile of the pyramidal cell

Current unit	Parameter values
C_m ($\mu F/cm^2$)	1.2
g_L (mS/cm^2)	0.02
E_L (mV)	−65
g_{Na} (mS/cm^2)	45
E_{Na} (mV)	55
g_{NaP} (mS/cm^2)	1
E_{NaP} (mV)	55
g_{Kd} (mS/cm^2)	18
E_{Kd} (mV)	−80
g_{HVA} (mS/cm^2)	1
E_{HVA} (mV)	120
g_{Ks} (mS/cm^2)	0.12
E_{Ks} (mV)	−80
g_{AHP} (mS/cm^2)	5
E_{AHP} (mV)	−80
K_d (μM)	30
γ($\mu M\,cm^2/ms/\mu A$)	0.002
$\tau_{Ca,AHP}$ (ms)	70
g_C (mS/cm^2)	80
E_C (mV)	−80
$\tau_{Ca,C}$ (ms)	10
$[Ca^{2+}]_o$ (mmol/lt)	2
$[Ca^{2+}]_{rest}$ (mmol/lt)	100e−3

Table 2
Parameter profile of the inhibitory interneuron

Current unit	Parameter values
C_{inj} ($\mu F/cm^2$)	1.2
g_L (mS/cm^2)	0.02
E_L (mV)	−65
g_{Na} (mS/cm^2)	45
E_{Na} (mV)	55
g_{Kd} (mS/cm^2)	18
E_{Kd} (mV)	−80

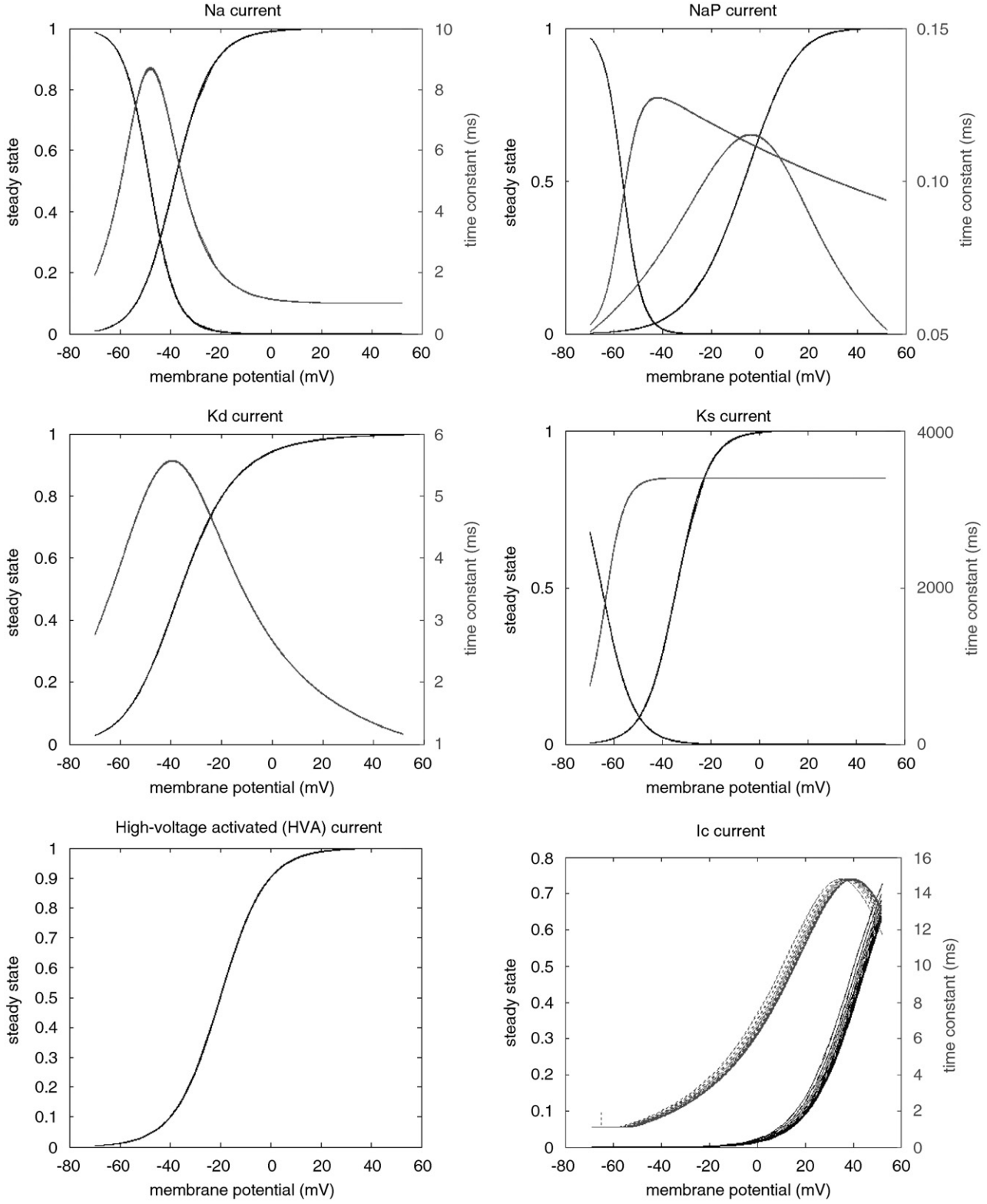

Fig. 2. Composite plot of activation and inactivation curves and their time constants for the model ionic channels. Membrane potential units are in mV. Time constant units are in ms.

where the normalized concentration of the postsynaptic transmitter–receptor complex, $F(V_{\text{pre}})$, is assumed to be an instantaneous and sigmoid function of the presynaptic membrane potential, $F(V_{\text{pre}})=1/(1+\exp(-(V_{\text{pre}}-\theta)/2))$, where $\theta_{\text{syn}}=0\,\text{mV}$ is high enough so that the transmitter release occurs only when the presynaptic cell emits a spike [36,49]. The values of the channel opening and closing rates are displayed in Table 3.

Table 3
Synaptic parameters

Synaptic current unit	g (mS/cm^2)	E (mV)	α (ms^{-1})	β (ms^{-1})
AMPA	4 [4–5.89]	0	12	0.2
NMDA	0.29 [0.05–0.29]	0	8	0.1
GABA-A	0.2 [0.2–5.6]	−75	12	0.2

Synaptic conductance values in brackets signify the normal range of synaptic conductances adapted from [13] and references therein.

2.3. Cortical network connectivity

The network model consists of N pyramidal neurons and M inhibitory interneurons ($M \approx N/3$) [1]. All four types of neuronal connectivity are allowed: pyramidal-to-pyramidal, pyramidal-to-inhibitory, inhibitory-to-pyramidal and inhibitory-to-inhibitory. All-to-all connectivity is assumed between inhibitory interneurons and between inhibitory interneurons and pyramidal neurons in the network (see Fig. 1).

In the model, the maximal synaptic conductance g_{syn} is estimated by dividing by a fixed average number of synaptic inputs per neuron, M_{syn}, so that when the number of synapses M_{syn} is varied, the total synaptic drive per cell in average remains the same [50].

2.4. Population firing rate

The population firing rate is defined as the fraction of neurons that are active in a short interval $[t, t+\Delta t]$ divided by Δt and it is estimated by

$$AF = \frac{n_{act}(t; t+\Delta t)}{\Delta t N}, \quad (6)$$

where n_{act} is the number of spikes in the time interval $[t, t+\Delta t]$, N is the total number of neurons in the network, and Δt is the size of the time bin [20].

2.5. Superior colliculus (SC) model

The SC model is a one-dimensional on-center off-surround leaky competitive integrator of the intermediate layer of the SC developed in another study by our group [10,11]. The neural architecture of the model is described in Fig. 1. Detailed description of the model and the equations that governed it can be found in [11].

2.6. Implementation

The simulations were performed on a Pentium IV 3.2 GHz PC with MATLAB's version R13 installed. The whole system of differential and algebraic equations was implemented in MATLAB (The MathWorks, Inc, Natick, MA). The differential equations of the cortical neural integrator model were integrated numerically using one of the MATLAB ordinary differential equations solvers (ode45, an implicit solver based on the Dormand–Prince pair method [41]) with time step $\Delta t = 0.001$ ms). Relative (error) tolerance was set to 10^{-6}.

3. Experimental results

3.1. Single neuron simulations

In response to a depolarizing current pulse, the model neuron initially fires at a high frequency, then adapts to a steady-state frequency (Fig. 3). This firing pattern is in parallel with the time course of Ca^{2+} accumulation [24]. The I_{AHP} increases with $[Ca^{2+}]$, hence the cell is gradually hyperpolarized and the firing frequency decreases in time. After the current pulse, there is a long-lasting AHP that mirrors the Ca^{2+} and hence the I_{AHP} decay (Fig. 3) [49].

In Fig. 4 a plot of the firing frequency versus the applied current intensity (f–I_{app} curve) of the model neuron is shown. It is noticeable that f–I curve is quite non-linear. The firing rate can be as high as 400 Hz [21,49].

Fig. 5 shows plots of the model's synapse. A brief current pulse is applied to the pre-synaptic cell, which generates a single action potential (see Fig. 5(A)), which in turn elicits an inhibitory postsynaptic current (I_{GABA}) and two excitatory postsynaptic currents (I_{AMPA} and I_{NMDA}) (see Fig. 5(B)).

3.2. Population neuron simulations

The two cortical network models simulated herein consisted of 15 pyramidal neurons and 5 inhibitory interneurons each. We assumed that the population firing rate of each cortical model represented the average firing rates of the frontal (e.g., frontal eye fields, FEF) and parietal (e.g., lateral intraparietal area, LIP) cortices. As we mentioned in the Materials and Methods Section, all four types of neuronal connectivity were allowed: pyramidal-to-pyramidal, pyramidal-to-inhibitory, inhibitory-to-pyramidal and inhibitory-to-inhibitory. Small cortical column connectivity (asymmetry) was examined in this study. That meant that the synaptic strength between pyramidal neurons inside the cortical column was maximal, whereas the synaptic strength between neurons inside and outside the column was 10% of g_{max} [15]. The number of pyramidal neurons in a cortical column was chosen arbitrarily based on a simple rule: $floor(N/2) - 2$, where N is the number of pyramidal neurons in the network. The reason we chose such a rule is because we wanted the cortical column to contain a sufficiently large number of heterogeneous neurons to produce a smooth population signal. We did not get into quantitative analysis of the cortical columns as in [5,6]. In this particular network, the number of pyramidal neurons in a cortical column was 5.

Furthermore, model pyramidal neurons and inhibitory interneurons were not identical. Heterogeneity in the network was induced by applying a depolarizing current I_{inj} of different intensity to each neuron and by varying the

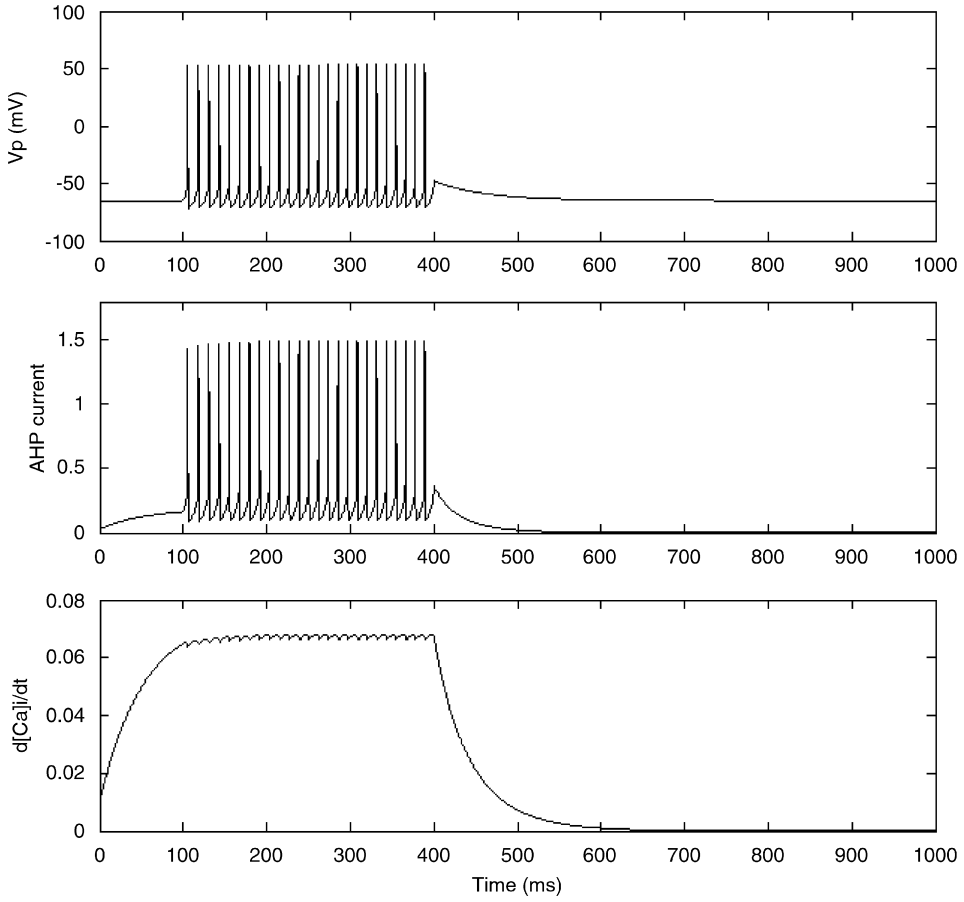

Fig. 3. Spike-frequency adaptation in response to a current pulse (not shown). Duration of the current pulse is 300 ms (100–400 ms). Each action potential generates a $[Ca^{2+}]$ influx and the adaptation time course follows that of $[Ca^{2+}]$ and hence I_{AHP} accumulation. Slow AHP after the spike firing mirrors the $[Ca^{2+}]$ decay process.

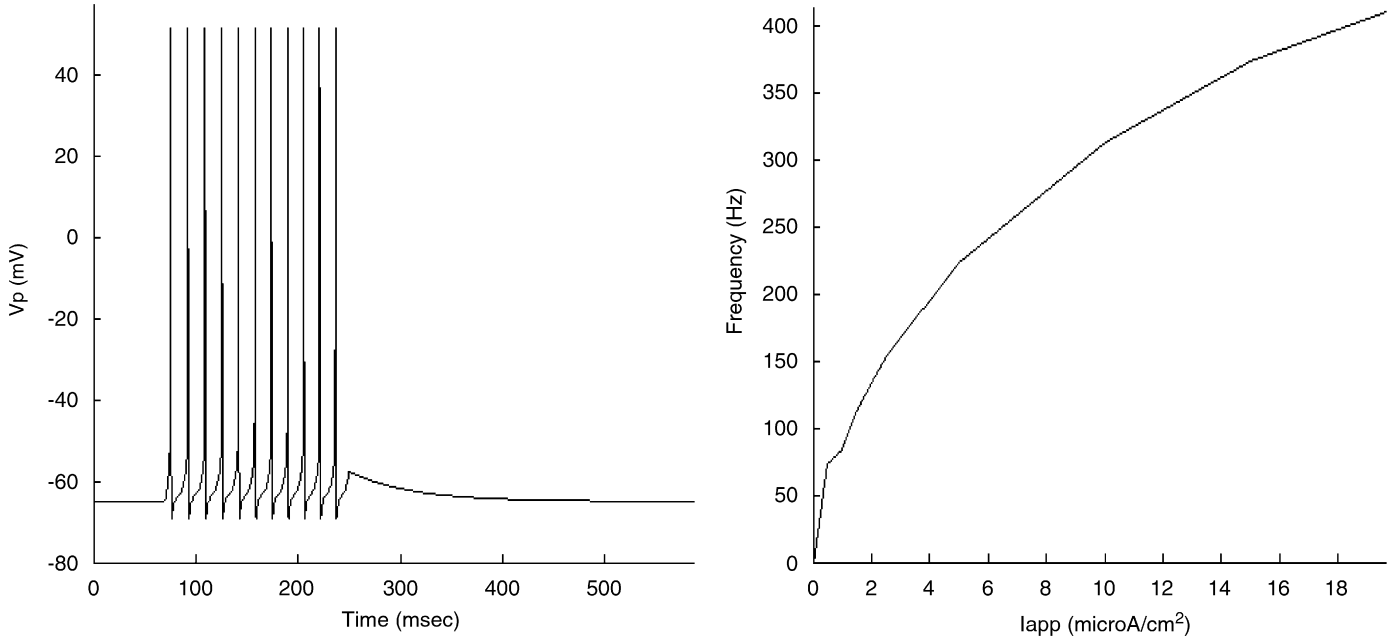

Fig. 4. Pyramidal cell firing and its frequency–current curve.

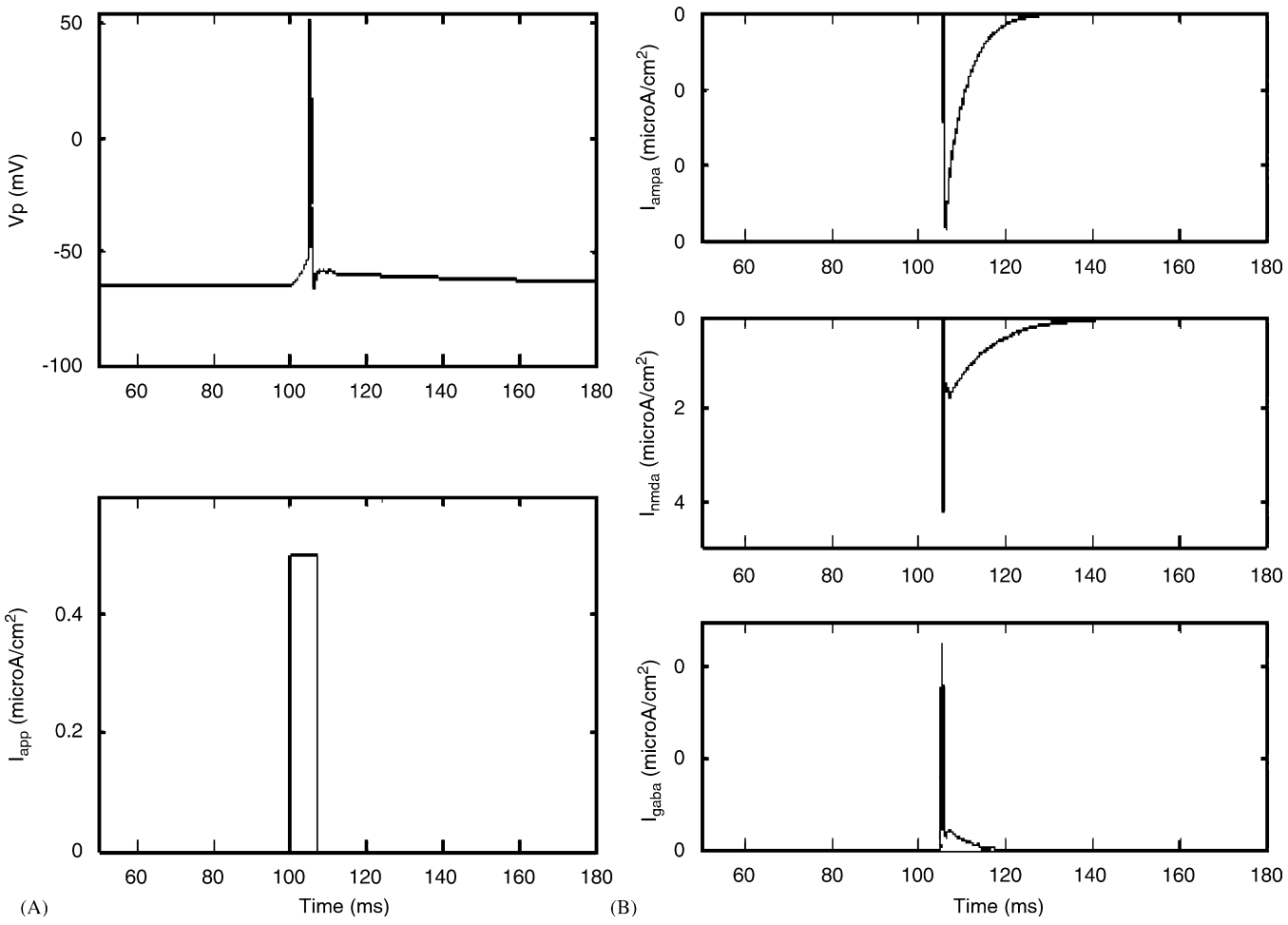

Fig. 5. Model of single neuron synapse. (A) A brief current pulse is applied to a presynaptic cell that generates a single action potential. (B) An inhibitory postsynaptic current ($I_{\mathrm{GABA-A}}$) and two excitatory postsynaptic currents (I_{AMPA} and I_{NMDA}) are elicited.

maximal synaptic conductances of each neuron. The injected current I_{inj} had a Gaussian distribution with mean I_{μ}^{inj} and a standard deviation$I_{\sigma}^{\mathrm{inj}}$. The parameter I_{μ}^{inj} determined the mean excitation be the external drive and $I_{\sigma}^{\mathrm{inj}}$ the degree of heterogeneity in the neuronal population. Similarly, the maximal conductances of the three synaptic currents (AMPA, NMDA and GABA-A) were allowed to vary randomly with means $g_{\max}^{\mathrm{AMPA}}$, $g_{\max}^{\mathrm{NMDA}}$, $g_{\max}^{\mathrm{GABA\text{-}A}}$ and standard deviations $g_{\sigma}^{\mathrm{AMPA}} = 0.05\,\mathrm{mS/cm^2}$, $g_{\sigma}^{\mathrm{NMDA}} = 0.05\,\mathrm{mS/cm^2}$, $g_{\sigma}^{\mathrm{GABA\text{-}A}} = 0.05\,\mathrm{mS/cm^2}$. The case of symmetrical neuronal connectivity and neuronal homogeneity was examined in another study from our group [9].

To estimate the population firing rate of each cortical model we divided the time axis into bins of 100 ms and summated in each bin the number of spikes. We then divided the total number spikes in each bin by the number of neurons in the network (see Eq. (6)). Fig. 6 shows the spiking rates of 3 pyramidal neurons and their estimated average population firing rate in a single run (trial). The output population firing rates of the two cortical networks can be used as inputs to the SC model.

In a recent study, Cutsuridis and colleagues [11] predicted that in order to quantitatively simulate the correct antisaccade and error prosaccade SRT distributions as well as the error probabilities in 10 virtual groups of 2006 subjects, two spatially separated and independent cortical decision signals were required as inputs to a neural model of the intermediate layer of the SC. In this model, the rising phases of the cortical decision signals were allowed to vary randomly from two normal distributions with different means and standard deviations for each of the 10 virtual groups of subjects (see Materials and Methods section of [11] on how clustering analysis was performed). Table 4 depicts the predicted values of the means and standard deviations of the cortical planned and reactive decision signals (mean values from all 10 groups range from 0.75 to 10.5) as well as the threshold values (450 ± 50 Hz) used to predict the range of correct and error SRTs and error rates from the Cutsuridis et al. study [11].

As we mentioned in the Introduction section, our goal in the present study is to model the cortical decision signals of the SC model [11] as outputs of two cortical networks consisting of pyramidal neurons and inhibitory interneurons and to examine the biophysical mechanisms that produce the variability in their rising phases. More specifically, we are interested in reproducing the full range

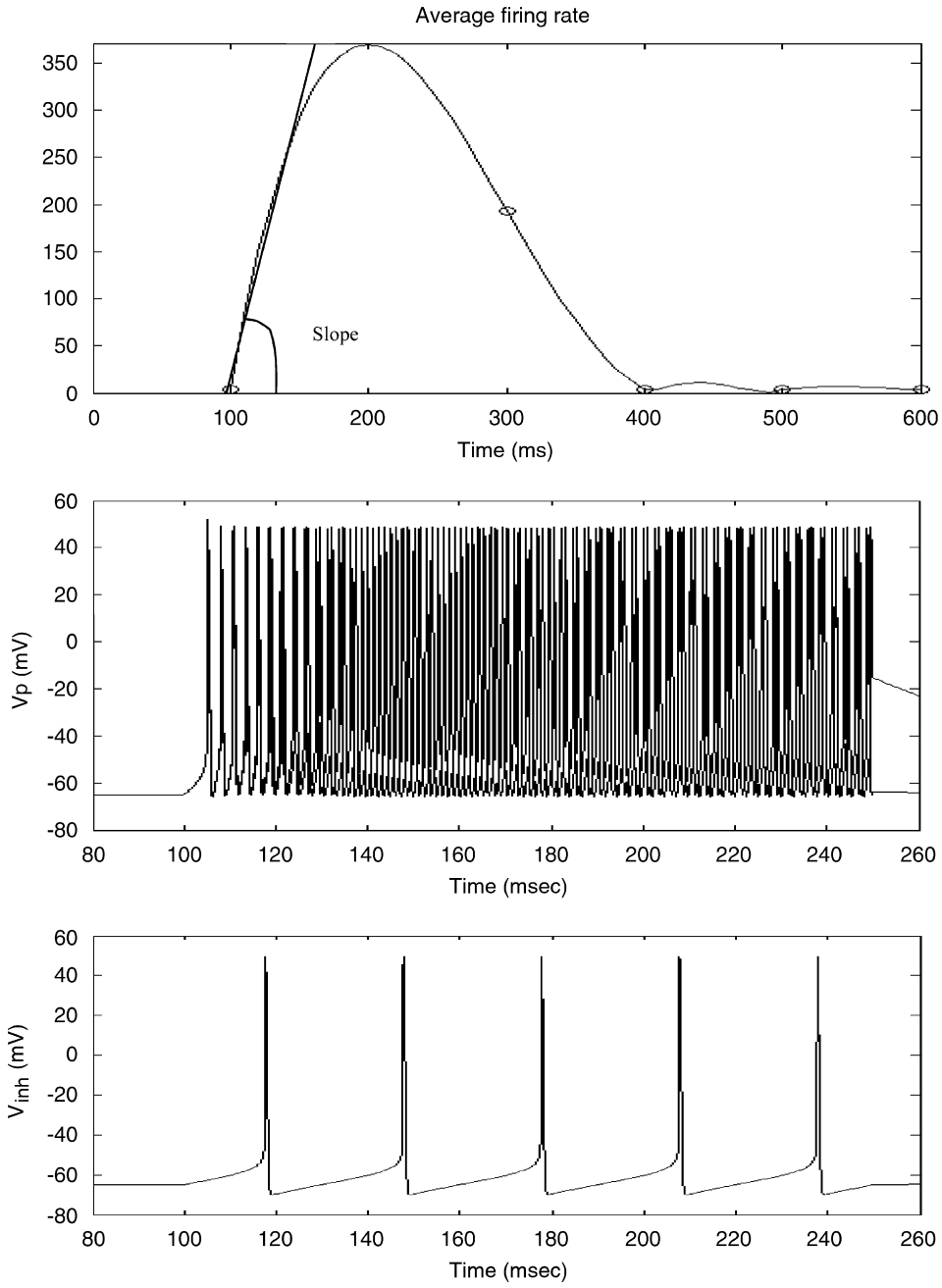

Fig. 6. (Top) Smooth spline fit of average firing rate of a heterogeneous population of 3 pyramidal and 1 inhibitory interneuron with asymmetrical connections; (Middle) Membrane potentials of three pyramidal neurons; (Bottom) Membrane potentials of one GABAergic interneuron. Time units are in ms.

of slope values (0.75–10.5) of the cortical input signals across all ten virtual groups, while keeping the preset threshold level fixed ($\sim 450 \pm 50$ Hz) (see Table 4). To do so, we performed detailed parametric analysis of the ionic and synaptic maximal conductances of all the currents used in our present's study model. We allowed the maximal conductances of all synaptic and ionic currents used in the model to vary (see Table 5 for conductance values of each current used). The maximal conductance values for each cell model were chosen to correspond to physiologically realistic values [2,4,8,15,26,27,44,45,46]. Conductance values in italics were considered as the basis conductance values [15]. If successful at reproducing the slope values depicted in Table 4, then we could implicitly say that we are able to generate the correct antisaccade and the error prosaccade RT distributions and the error probabilities in a large group of 2006 men [16,43] published elsewhere [11].

In our parametric analysis, we initially allowed the maximal conductance of each current to vary separately, while we kept the conductances of all other currents to their basis values (see italics values). For each different value of the maximum conductance, we estimated the

Table 4
Mean and standard deviation of slopes of planned and reactive inputs, simulated correct median, error median, and error rate for average and all ten groups and values of χ^2 test of homogeneity between correct and error experimental and simulated percent density distributions for antisaccades and error prosaccades

	μ_1	σ_1	μ_2	σ_2	Threshold	Median RT of antisaccades	Median RT of error prosaccades	Percent antisaccade error rate	Antisaccades	Error prosaccades
Group 1	4.0	1.0	3.6	0.9	416	294.174 (288.16)	279.541(265.20)	13.04 (16.15)	36.15	34.92
Group 2	3.6	1.0	5.3	1.5	392	276.50 (279.21)	202.97 (201.96)	38.62 (39.07)	90.5*	33.56
Group 3	3.5	0.9	5.5	1.6	400	281.89 (280.91)	212.54 (201.92)	20.15 (23.73)	32.16	32.89
Group 4	4.9	1.3	5.8	1.5	400	251.30 (249.27)	209.90 (211.65)	12.41 (12.02)	56.06*	96.24*
Group 5	4.7	1.8	5.0	1.3	408	254.80 (242.40)	212.99 (216.66)	24.27 (17.02)	35.21	24.18
Group 6	3.4	0.8	6.8	1.8	384	282.38 (288.44)	188.10 (193.66)	23.93 (28.86)	31.82	27.97
Group 7	3.9	0.9	7.5	2.0	376	263.10 (251.79)	180.63 (175.53)	20.87 (24.79)	30.34	21.82
Group 8	2.1	0.5	4.6	1.3	406	365.69 (349.42)	218.99 (221.36)	37.00 (34.58)	36.46	35.67
Group 9	7.3	2.3	7.5	2.1	367	218.20 (213.58)	177.85 (172.77)	27.36 (24.92)	36.99	23.15
Group 10	2.8	0.9	2.4	0.6	432	327.56 (307.5)	331.07 (326.99)	20.05 (21.81)	33.88	83.57*
All subjects	3.7	0.8	5.9	1.6	493	274.75 (275.07)	198.61 (200.67)	21.53 (24.3)		

Values in parentheses stand for experimental values (table adapted from unpublished observations [11]).
Units: correct SRT (ms), error SRT (ms). χ^2 values marked with an asterisk indicate a significant difference between the simulated and the observed RT distributions. *Rejection region*: $\chi^2 \geqslant \chi^2_{0.05}(37.65)$.
The degrees of freedom were 25.
Mean values from all groups range approximately from 0.75–10.5.

Table 5
List of ionic and synaptic parameters varied in the model to produce varying climbing activity

Current unit	g (mS/cm^2)
Pyramidal neuron	
I_{AMPA}	*4*, 4.5, 5, 5.5, 5.9
I_{NMDA}	0.05, 0.1, 0.2, *0.29*
I_{GABA-A}	*0.2*, 0.5, 1, 1.5, 2.5, 3, 4, 5, 5.5
I_{NaP}	0.05, 0.1, 0.5, *1*, 2, 5, 10, 30, 50
I_{Kd}	8, *18*, 28, 58, 78, 108, 138, 158
I_{Ks}	0.05, 0.1, *0.12*, 0.2, 0.5, 1, 2, 3, 5, 10, 20, 50, 100
I_C	1, 5, 10, 30, 50, *80*, 100, 150
I_{AHP}	0.5, 1, 3, *5*, 7, 10, 50, 100, 150
I_{HVA}	0.05, 0.1, 0.5, *1*, 2, 5, 8
Inhibitory interneuron	
I_{AMPA}	*4*, 4.5, 5, 5.5, 5.9
I_{NMDA}	0.05, 0.1, 0.2, *0.29*
I_{GABA-A}	*0.2*, 0.5, 1, 1.5, 2.5, 3, 4, 5, 5.5

Conductance values in italics are considered as the basis conductance values [15].

network's population firing rate and subsequently its slope. To estimate the slope, we fitted a straight line on the rising phase of each population firing rate and calculated the angle the straight line with the *x*-axis (time) (see Fig. 6). From all the synaptic and ionic currents used in our parametric analysis, only the I_{Kd}, I_{NaP}, I_{HVA}, I_{AMPA}, and I_{NMDA} were found to produce changes in the slopes of the climbing activities of the cortical signals. From these currents, I_{HVA} and I_{Kd} were able to produce the entire range of slope values observed in Table 4. However, I_{HVA} and I_{Kd} caused the maximal neuronal population firing rate to also vary (ranging from about 50 to 500 Hz) between different conductance value runs (see Fig. 7 top). Hanes and Schall [23] showed that while the climbing activities of FEF neurons vary randomly from trial to trial, their maximum firing rate remains constant. Similarly, Cutsuridis and colleagues [11] predicted that the maximum neuronal firing rate and hence the threshold level remain constant from trial to trial in each virtual group, while the threshold level varies slightly (about $\pm$50 Hz) around its maximum value ($\sim$450 Hz) between virtual groups. For these reasons, we excluded I_{HVA} and I_{Kd} currents from any further examination.

Parametric examination of I_{NaP}'s maximal conductance produced the entire range of slope values of the climbing activities seen in Table 4, whereas parametric examination of I_{AMPA}, and I_{NMDA} produced a subset of them. For the different values of these currents' conductances, the maximal cortical neuronal firing rate remained unaffected ($\sim$450 Hz).

The final step was to try combinations of maximal conductance values of the I_{NaP}, I_{AMPA}, and I_{NMDA}. We found that the range of values of maximal conductances of these currents that produce the full range of slope values

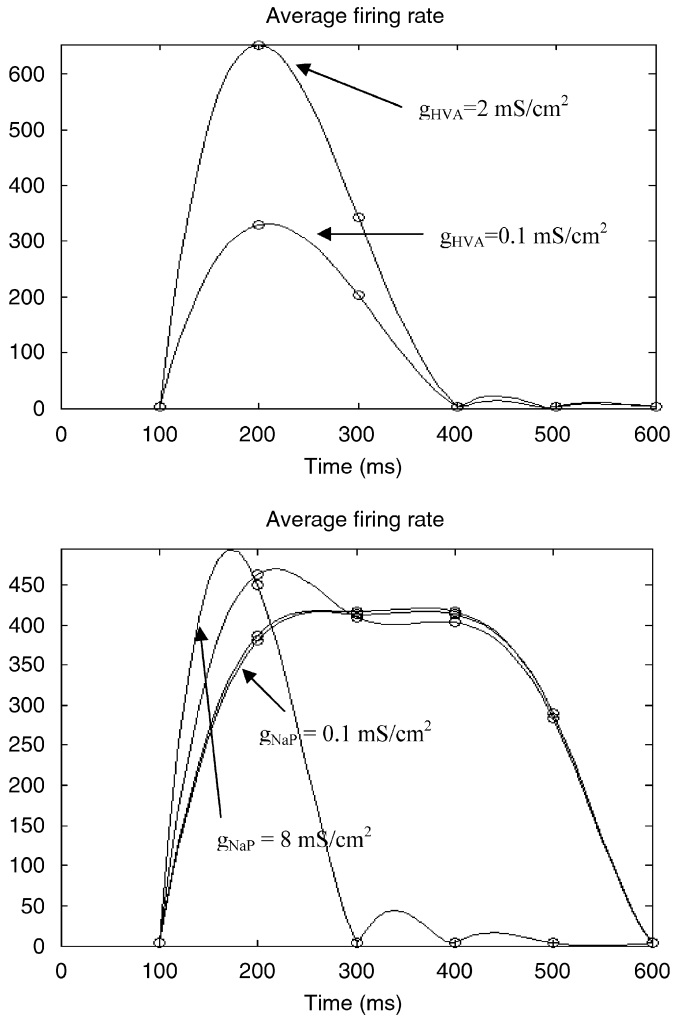

Fig. 7. (Top) Composite smooth spline fits of average firing rate of a heterogeneous population of 15 pyramidal neurons and 5 inhibitory interneurons with asymmetrical connections for different values of g_{HVA}. Note that maximal population firing rate varies between 50 and 650 Hz for 0.1 and 2 mS/cm^2 HVA conductance, respectively; (Bottom) Composite smooth spline fits of average firing rate of a heterogeneous population of 15 pyramidal neurons and 5 inhibitory interneurons with asymmetrical connections for different values of g_{NaP}. Note that maximal population firing rate varies between 450 ± 50 Hz for 0.1 and 8 mS/cm^2 NaP conductance, respectively.

(0.75–10.5 rad from all 10 virtual groups) of climbing activities and the fixed threshold ($\sim 450 \pm 50$ Hz) for all 10 virtual groups (see Fig. 7 bottom) observed in Table 4 were: I_{NaP} (mS/cm^2): 0.05, 0.1, 0.5, 1, 2, 5, 10, 30; I_{AMPA} (mS/cm^2): 4, 4.5, 5, 5.5, 5.9; I_{NMDA} (mS/cm^2): 0.05, 0.1, 0.2, 0.29.

4. Discussion

4.1. General issues

In the brain, climbing activity is a very prominent profile of neuronal activity observed in the thalamus, FEFs, primary motor cortex, SC and other brain areas and it has been found to be related to the anticipation of forthcoming events and to the generation of movements [13]. In the FEFs of monkeys populations of visuomotor neurons have been found that begin to fire in advance of saccades, with their activity rising linearly upon presentation of a suitable target stimulus [23,39]. The primary function of these neurons is to make preparations for saccadic eye movements [23]. Buildup cells in the monkey SC begin to linearly build up their activity after the signal to make a saccade is presented [17]. In all these studies, the rate of rise varies randomly from trial to trial and the saccade is initiated when this activity reaches a fixed threshold [23,39].

4.2. Previous models

Very few models have tried to address important questions concerning the climbing activity of neurons in the cortex. Okamoto and Fukai [37] addressed the question of what produces the linearity of the climbing activity in a population of cortical neurons and showed that inputs to FEFs or supplementary eye fields from the visual cortex is possible to be modified by attention that can easily be varied across trials. However, their model was too simplistic since they modeled only two currents, namely the ionic ADP and the synaptic AMPA currents.

In another study, Reutimann and colleagues [40] advanced a general model of interacting neuronal populations that generated event-based representation of time by slowly increasing (climbing) activity and suggested a functional role for the climbing activity of inferotemporal (IT) neurons. Although their model was successful at simulating this particular set of behavioral data, they failed to identify the ionic and synaptic mechanisms of the slowly increasing climbing activity.

Durstewitz [13,14] has recently offered a plausible hypothesis of what might produce variability in the rising rates of a decision signal. He advanced a biophysical model that produced temporal integrator-like activity with variable slopes, through a single-cell positive feedback loop between firing rate, spike-driven Ca^{2+} influx, and Ca^{2+}-activated inward currents. In the model the self-organizing process was based on observations that the variance of the intracellular Ca^{2+} concentration and the variance of the neural firing rate and of activity-dependent conductances reach a maximum as the biophysical parameters of the neuron approached a configuration required for temporal integration. However, the response times produced by this model were of the order of several hundred milliseconds to seconds, whereas the RTs in the antisaccade task range from tens to few hundreds of milliseconds.

All three studies were successful in their own respect, but none of them has attempted to answer the questions of what are the biophysical mechanisms underlying the generation of variable temporal integrator behavior and how these mechanisms are related to behavior. These questions are successfully addressed by our model.

4.3. What have we learned from the model?

The model presented herein offers an alternative theoretical view on biologically plausible biophysical mechanisms underlying the generation of slowly climbing, temporal integrator-like activity found in the neocortex [23,39]. It simulates accurately the neuronal responses of pyramidal neurons and inhibitory interneurons by incorporating in its equations a wealth of ionic and synaptic currents found experimentally in the cortex [47]. We chose to model these particular ionic currents, because they are the main representatives (families) of the cortical ionic currents and because their properties have been studied extensively in the lab [2,4,30–32,49,51] as well as computationally modeled [15,51]. The model in addition to computational findings of previous studies from our group [9–11] is capable of producing time intervals of the order of tens up to few hundred of milliseconds, as they are observed in the antisaccade task [16,43].

The model makes two important predictions. First, it is successful at predicting that variability *only* in the maximal conductances of ionic I_{NaP} and synaptic I_{AMPA}, and I_{NMDA} currents, and *not in any other currents* used in the model, can produce the predicted full range of variability of climbing activities as well as their maximal firing rate of two independent and spatially separated cortical decision signals needed to drive a SC model [11] and, hence, implicitly predict the correct antisaccade and the error prosaccade RT distributions as well as response probabilities in all 10 virtual groups of subjects (see Table 4; [11]). Second, the model predicts the ranges of values of I_{NaP}, I_{AMPA}, and I_{NMDA} conductances, which are *verified* by patch clamp studies [2,4,8,15,26,27,45,46], needed to produce the full range of slope values of the climbing activities of the decision signals.

We believe that both predictions are equally important that ought to be verified experimentally in vivo by the experimental scientists of the brain with the use of agonists and antagonists that will modulate (enhance or partially block, respectively) the conductances of the ionic and synaptic currents used in the model as well as with the use of neuromodulators such as dopamine or acetylcholine, and *simultaneously* record via single cell recordings their effects on the neuronal responses of cortical neurons of *awake* and *behaviorally* involved animals.

4.4. Future extensions

Work is underway in our laboratory to extend the present work and examine the effects of neurotransmitters such as dopamine (DA) on the *predicted* synaptic (I_{AMPA} and I_{NMDA}) and ionic (I_{NaP}) conductances of pyramidal neurons in the two cortical networks in order to study the performances of patients suffering from schizophrenia in the antisaccade task [28]. Briefly, in that study we try to show how the effect of DA-D1 can affect the cortical modules by acting directly on the receptors of the cells and hence modify the currents of these modules. The action of DA-D1 on the cortical modules is effectively modifying the profile of their spiking rate and subsequently of their average firing rate and hence critically changes the behavior of these populations of cells. We have successfully simulated three different levels of DA (hypo, normal, and hyper) to study its effects on the rising phases of the cortical decision signals and observed that the simulated aSRTs for the hypo-DA level, representing the schizophrenic group had higher standard deviations, mean values, error rates and coefficient of variation than in normal and hyper DA level [28,29]. This finding comes in perfect agreement with our psychophysical observations [28,29].

Also, another line of research that our group is currently pursuing and that extends the previous work [28,29] is the study of if there are any effects of DA-D2 receptors on the neuronal responses of pyramidal neurons in the cortical modules and subsequently on the behavioral data of the patient group mentioned before.

Finally, we are examining the effects of DA on ionic and synaptic mechanisms of cortical GABAergic inhibitory interneurons, their role in the cortical microcircuit [42], how their neuronal excitability affects the responses of pyramidal neurons and subsequently the population climbing activity of the cortical modules. The last line of research will help generalize our model, make new predictions (if any), and suggest new experiments.

References

[1] M. Abeles, Local cortical circuits, Springer, Berlin Heidelberg, New York, 1982.
[2] C. Alzheimer, P.C. Schwindt, W.E. Crill, Modal gating of Na^+ channels as a mechanism of persistent Na^+ current in pyramidal neurons from rat and cat sensorimotor cortex, J. Neurosci. 13 (2) (1993) 660–673.
[3] A.M. Brown, P.C. Schwindt, W.E. Crill, Voltage dependence and activation kinetics of pharmacologically defined components of the high-threshold current in rat neocortical neurons, J. Neurophys. 70 (1993) 1530–1543.
[4] A.M. Brown, P.C. Schwindt, W.E. Crill, Different voltage dependence of transient and persistent Na^+ currents is compatible with modal-gating hypothesis for sodium channels, J. Neurophysiol. 71 (6) (1994) 2562–2565.
[5] D.P. Buxhoeveden, A.E. Switala, E. Roy, M.F. Casanova, Quantitative analysis of cell columns in the cerebral cortex, J. Neurosci. Meth. 97 (2000) 7–17.
[6] D. Chklovskii, Synaptic connectivity and neuronal morphology: two sides of the same coin, Neuron 43 (5) (2004) 609–617.
[7] C. Condy, S. Rixaud-Pechoux, F. Ostendorf, C.J. Ploner, B. Gaynard, Neural substrate of antisaccades: role of subcortical neurons, Neurology 63 (9) (2004) 1571–1578.
[8] T.R. Cummins, Y. Xia, G.G. Haddad, Functional properties of rat and human neocortical voltage-sensitive sodium currents, J. Neurophysiol. 71 (3) (1994) 1052–1064.
[9] V. Cutsuridis, I. Kahramanoglou, S. Perantonis, I. Evdokimidis, N. Smyrnis, A biophysical neural model of decision making in an antisaccade task through variable climbing activity, in: artificial neural networks: biological inspirations—ICANN '05, lecture notes in computer science, vol. 3696, Springer, Berlin, 2005, pp. 205–210.

[10] V. Cutsuridis, N. Smyrnis, I. Evdokimidis, I. Kahramanoglou, S. Perantonis, Neural network modeling of eye movement behavior in the antisaccade task: validation by comparison with data from 2006 normal individuals, in: Program No. 72.13. 2003 Abstract Viewer/ Itinerary Planner, Society for Neuroscience, Washington, DC, 2003.
[11] V. Cutsuridis, N. Smyrnis, I. Evdokimidis, S. Perantonis, A neural model of decision making by the superior colliculus in an antisaccade task, *under review Neural Networks*.
[12] A. Destexhe, Z.F. Mainen, T.J. Sejnowski, An efficient method for computing synaptic conductances based on a kinetic model of receptor binding, Neural Comp. 6 (1994) 14–18.
[13] D. Durstewitz, Self organizing neural integrator predicts interval times through climbing activity, J. Neurosci. 23 (12) (2003) 5342–5353.
[14] D. Durstewitz, Neural representation of interval time, Neuroreport 15 (9) (2004) 745–749.
[15] D. Durstewitz, J.K. Seamans, T.J. Sejnowski, Dopamine-mediated stabilization of delay-period activity in a network model of prefrontal cortex, J. Neurophys. 83 (2000) 1733–1750.
[16] I. Evdokimidis, N. Smyrnis, T.S. Constantinidis, N.C. Stefanis, D. Avramopoulos, C. Paximadis, C. Theleritis, C. Efstratiadis, G. Kastrinakis, C.N. Stefanis, The antisaccade task in a sample of 2006 young men I. normal population characteristics, Exp Brain Res 147 (2002) 45–52.
[17] S. Everling, M.C. Dorris, R.M. Klein, D.P. Munoz, Role of primate superior colliculus in preparation and execution of anti-saccades and prosaccades, J. Neurosci. 19 (7) (1998) 2740–2754.
[18] S. Everling, M.C. Dorris, R.M. Klein, D.P. Munoz, Role of primate superior colliculus in preparation and execution of anti-saccades and pro-saccades, J. Neurosci. 19 (7) (1998) 2740–2754.
[19] S. Everling, B. Fischer, The antisaccade: a review of basic research and clinical studies, Neuropsychologia 36 (1998) 885–899.
[20] W. Gerstner, W. Kistler, Spiking Neuron Models, Cambridge University Press, Cambridge, UK, 2002.
[21] B.S. Gutkin, C.R. Laing, C.L. Colby, C.C. Chow, G.B. Ermentrout, Turning on and off with excitation: the role of spike-timing asynchrony and synchrony in sustained neural activity, J. Comp. Neurosci. 11 (2001) 121–134.
[22] P.R. Hallett, Primary and secondary saccades to goals defined by instructions, Vision Res. 18 (1978) 1279–1296.
[23] D.P. Hanes, J.D. Schall, Neural control of voluntary movement initiation, Science 274 (1996) 427–430.
[24] F. Helmchen, K. Imoto, B. Sakmann, Ca^{2+} buffering and action potential-evoked Ca^{2+} signalling in dendrites of pyramidal neurons, Biophys. J. 70 (1996) 1069–1081.
[25] A.L. Hodgkin, A.F. Huxley, A quantitative description of membrane current and its application to conduction and excitation in nerve, J. Physiol. 117 (4) (1952) 500–544.
[26] J.R. Huguenard, D.A. Coulter, D.A. Prince, A fast transient potassium current in thalamic relay neurons: kinetics of activation and inactivation, J. Neurophysiol. 66 (4) (1991) 1304–1315.
[27] J.R. Huguenard, D.A. Prince, Slow inactivation of a TEA-sensitive K^+ current in acutely isolated rat thalamic relay neurons, J. Neurophysiol. 66 (4) (1991) 1316–1328.
[28] I. Kahramanoglou, V. Cutsuridis, N. Smyrnis, I. Evdokimidis, S. Perantonis, Dopamine modification of climbing activity in a neural accumulator model of the antisaccade task, in: Proceedings of the First Computational Cognitive Neuroscience Conference, New Orleans, USA, 2005.
[29] I. Kahramanoglou, V. Cutsuridis, N. Smyrnis, I. Evdokimidis, S. Perantonis, Dopamine effects on climbing activity of a cortico-tectal model: simulating the performance of patients with DSM-IV schizophrenia in the antisaccade task, In: 2nd Computational Cognitive Neuroscience Conference, Houston, TX, USA, November 16–19, 2006.
[30] A.R. Kay, R.K.S. Wong, Calcium current activation kinetics in isolated pyramidal neurones in the CA1 region of the mature guinea-pig hippocampus, J. Physiol. (Lond), 392 (1987) 603–616.
[31] C. Koch, Biophysics of computation: information processing in single neurons, Oxford University Press, Oxford, UK, 1999.
[32] R. Latorre, A. Oberhauser, P. Labarca, O. Alvarez, Varieties of calcium-activated potassium channels, Ann. Rev. Physiol. 51 (1989) 385–399.
[33] A. Moschovakis, A. Karabelas, Observations on the somatodedritic morphology and axonal trajectory of intracellularly HRP-labeled efferent neurons located in the deeper layers of the superior colliculus of the cat, J. Comp. Neurol. 239 (1985) 276–308.
[34] D. Munoz, R. Wurtz, Fixation cells in monkey superior colliculus. i. characteristics of cell discharge, J. Neurophysiol. 70 (1993) 559–575.
[35] D. Munoz, R. Wurtz, Saccade related activity in monkey superior colliculus. I. characteristics of burst and buildup cells, J. Neurophysiol. 73 (1995) 2313–2333.
[36] D. Munoz, R. Wurtz, Saccade related activity in monkey superior colliculus. II. spread of activity during saccades, J. Neurophysiol. 73 (1995) 2334–2348.
[37] H. Okamoto, T. Fukai, Neural bases of accumulator models, Neurocomputing 52–54 (2003) 285–288.
[38] A.A. Prinz, C.P. Billimoria, E. Marder, Alternative to hand-tuning conductance-based models: construction and analysis of databases of model neurons, J. Neurophysiol. 90 (2003) 3998–4015.
[39] B.A.J. Reddi, R.H.S. Carpenter, The influence of urgency on decision time, Nat. Neurosci. 3 (2000) 827–831.
[40] J. Reutimann, V. Yakovlev, S. Fusi, W. Senn, Climbing neuronal activity as an event-based cortical representation of time, J. Neurosci. 24 (13) (2004) 3295–3303.
[41] L.F. Shampine, M.W. Reichelt, The MATLAB ODE Suite, SIAM Journal on Scientific Computing 18 (1997) 1–22.
[42] G. Silberberg, S. Grillner, F.E.N. LeBeau, R. Maex, H. Markram, Synaptic pathways in neural microcircuits, Trends Neurosci. 28 (10) (2005) 541–551.
[43] N. Smyrnis, I. Evdokimidis, N.C. Stefanis, T.S. Constantinidis, D. Avramopoulos, C. Theleritis, C. Paximadis, C. Efstratiadis, G. Kastrinakis, C.N. Stefanis, The antisaccade task in a sample of 2006 young males II. effects of task parameters, Exp. Brain Res. 147 (2002) 53–63.
[44] J.F. Storm, Temporal integration by a slowly inactivating K^+ current in hippocampal neurons, Nature 336 (1988) 379–381.
[45] W.J. Spain, P.C. Schwindt, W.E. Crill, Two transient potassium currents in layer V pyramidal neurons from cat sensorimotor cortex, J. Physiol. 434 (1991) 591–607.
[46] W.J. Spain, P.C. Schwindt, W.E. Crill, Post-inhibitory excitation and inhibition in layer V pyramidal neurons from cat sensorimotor cortex, J. Physiol. 434 (1991) 609–626.
[47] M. Toledo-Rodriguez, A. El. Marina, P. Wallen, G. Svirskis, J. Hounsgaard, Cellular signaling properties in microcircuits, Trends Neurosci 28 (10) (2005) 534–540.
[48] D. Waitzman, T. Ma, L. Oprican, R. Wurtz, Superior colliculus neurons mediate the dynamic characteristics of saccades, J. Neurophysiol. 66 (1991) 1716–1737.
[49] X.J. Wang, Calcium coding and adaptive temporal computation in cortical pyramidal neurons, J. Neurophysiol. 79 (1998) 1549–1566.
[50] X.J. Wang, G. Buzsaki, Gamma oscillation by synaptic inhibition in a hippocampal interneuronal network model, J. Neurosci. 16 (20) (1996) 6402–6413.
[51] E.N. Warman, D.M. Durand, G.L.F. Yuen, Reconstruction of hippocampal CA1 pyramidal cell electrophysiology by computer simulation, J. Neurophysiol. 71 (6) (1994) 2033–2045.

Vassilis Cutsuridis is a research associate at the Computational Intelligence Laboratory of the Institute of Informatics and Telecommunications of N.C.S.R. "Demokritos". He has received a B.S. in physics and mathematics and an M.Sc. in theoretical physics from Wichita State University (USA), an MA. in Cognitive and Neural Systems from Boston University (USA) and a Ph.D. in Computational Cognitive Neuroscience from the National University of Athens (Greece). He has

worked for many years in the IT industry in Greece and US as a software engineer and a consultant. His research interests are in computational neuroscience, distributed systems, theory of neural networks, image processing and time series analysis.

Ioannis Kahramanoglou was born in Athens 1976, graduated from Oxford University in 1997 (BA in physics, MA in physics). Upon returning to Greece he studied condensed matter physics (National University of Athens) where he graduated in 2002 (Postgraduate degree). Currently he is working on his Ph.D. thesis on biologically inspired neural models of schizophrenia. He is a member of Computational Intelligence Laboratory of the National Centre for Scientific Research "Demokritos".

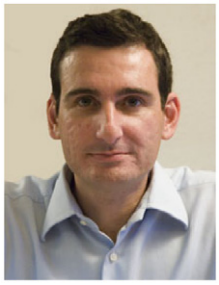

Nikolaos Smyrnis is a Lecturer in the Department of Psychiatry of the National and Kapodistrian University of Athens. Dr Smyrnis received his Ph.D. from the same University and has done post doctoral work in Johns Hopkins University USA and University of Minnesota USA. His main interest is the control of eye and arm movements in cognitive tasks. He has formed a research group with Prof. I Evdokimidis the "Cognition and Action Group" and is doing research on the above subject using psychophysical, electrophysiological and functional imaging methods.

Ioannis Evdokimidis is an Associate Professor in the Department of Neurology of the National and Kapodistrian University of Athens. His main interest is the control of eye and arm movements in cognitive tasks. He has formed a research group with Prof. Nikolaos Smyrnis the "Cognition and Action Group" and is doing research on the above subject using psychophysical, electrophysiological and functional imaging methods.

Stavros J. Perantonis is the holder of a B.S. degree in Physics from the Department of Physics, University of Athens, an M.Sc. degree in Computer Science from the Department of Computer Science, University of Liverpool and a D. Phil. Degree in Computational Physics from the Department of Physics, University of Oxford. Currently he holds the position of Senior Researcher and Head of the Computational Intelligence Laboratory. His current technical and research activities are in the areas of computational intelligence, neural networks and modelling, pattern recognition and multimedia processing. Dr. Perantonis is the author or co-author of over 100 papers in international journals and conference proceedings. He has managed or participated in many EU or nationally funded projects, mainly involving research into computational intelligence methods/algorithms and their application to industry, bio-medicine, finance, the environment and the world-wide-web.